

## CONFIRMATION AND CHARACTERIZATION OF GALACTIC PLANETARY NEBULAE: INSIGHTS FROM A SPECTROSCOPIC STUDY

D. A. Beleño-Molina,<sup>1</sup> L. Olguín,<sup>1</sup> L. F. Miranda,<sup>2</sup> M. E. Contreras,<sup>1</sup> and R. Vázquez<sup>3</sup>

*Draft version: April 9, 2025*

### RESUMEN

Presentamos un estudio espectroscópico de 25 objetos reportados como posibles Nebulosas Planetarias (NPs) en catálogos recientes para obtener sus propiedades físicas y establecer su verdadera naturaleza. Encontramos 11 objetos que muestran líneas de emisión intensas, 11 donde no fue posible medir H $\beta$  y tres que no muestran líneas. Utilizando diagramas de diagnóstico, hemos podido confirmar ocho objetos como verdaderas NPs. Para tres de estos objetos hemos determinado abundancias elementales que concuerdan con los valores del conjunto de NPs de nuestra Galaxia. Cuatro objetos muestran la línea [N II]  $\lambda$ 6583 más intensa que H $\alpha$  que puede explicarse en dos de ellos con la presencia de choques en el gas. Finalmente, reportamos tamaños angulares determinados a partir de la emisión en H $\alpha$  y [O III]  $\lambda$ 5007.

### ABSTRACT

We present a spectroscopic investigation of 25 objects previously reported as possible Planetary Nebulae (PNe) in recent catalogs to obtain their physical properties and to establish their true nature. We found 11 objects showing intense emission lines, 11 where it was not possible to measure H $\beta$ , and three where no lines are present. We have used diagnostic diagrams to confirm the true PN nature for eight objects. We obtained elemental abundances for three objects whose values are in agreement with the PNe mean values for our Galaxy. Four objects show [N II]  $\lambda$ 6583 more intense than H $\alpha$ , and for two of them, this can be explained by the presence of shocks in the gas. Finally, we report angular sizes based on H $\alpha$  and [O III]  $\lambda$ 5007 emission.

*Key Words:* Catalogues — ISM: Abundances — Planetary nebulae: General — Techniques: Spectroscopic

### 1. INTRODUCTION

Planetary Nebulae (PNe) are the product of the gas ejection of evolved stars with low and intermediate-mass progenitors ( $\sim 0.8\text{--}8M_{\odot}$ ). These stars eject the most external layers of their surface at the Asymptotic Giant Branch

---

<sup>1</sup>Departamento de investigación en Física, Universidad de Sonora (UNISON), Mexico.

<sup>2</sup>Instituto de Astrofísica de Andalucía (IAA), Consejo Superior de Investigaciones Científicas (CSIC), Spain.

<sup>3</sup>Instituto de Astronomía en Ensenada, Universidad Nacional Autónoma de México (UNAM), Mexico.

(AGB) evolutionary stage, with mass loss rates around  $10^{-8} M_{\odot} \text{ yr}^{-1}$ . At the tip of the AGB phase, mass loss reaches up to  $10^{-4} M_{\odot} \text{ yr}^{-1}$ , creating an expanding shell around them (Randall et al. 2020). When the uncovered central hot core reaches an effective temperature ( $T_{\text{eff}}$ ) of approximately 30,000 K (Khushbu & Muthumariappan 2024), it produces energetic photons capable of exciting and ionizing the previously ejected material, forming a so-called planetary nebula (PN). Subsequent line deexcitation and recombination in the envelope produce the characteristic spectrum associated with these objects (Osterbrock & Ferland 2006). Considering a scenario where single and binary stars produce PNe, the predicted Galactic population of these objects is about 46,000 (Moe & De Marco 2006). However, by 2000, the number of known PNe was approximately 1500 (Kohoutek 2001), much smaller than expected. More recently, as of April 2025, the Galactic known PNe population has increased to 3952 objects according to the HASH (Parker et al. 2016), an amount larger than the previous findings but still smaller than expected. This discrepancy could be explained by a high dust obscuration in the Galactic plane, by the faintness of old PNe or by the compactness of sources usually identified as stars (Kwok 2000).

During the last 20 years, many sky surveys have searched for these elusive objects, making a golden age of PNe discovery (Kwitter & Henry 2022; Parker 2022). Objects included in these catalogs generally have a small angular extent and some of them are underrepresented by its low surface brightness. Several authors have begun studying these objects (e.g. Henry et al. 2010; Acker et al. 2012; Hsia & Zhang 2014; Ali et al. 2016; Ritter et al. 2023; Temiz et al. 2024) but a considerable number (~1000) still need an initial study or a deeper analysis of their properties. Since these objects are poorly studied in literature, it is necessary to establish their true nature to understand if they could represent an evolutionary stage not well-studied before and why many of them were difficult to detect. The presence of dust, highly evolved objects, or small size emission regions can be claimed responsible for the latter.

Only some of the new objects reported in recent catalogs have been confirmed as true PNe (Sabin et al. 2014). Furthermore, additional studies are needed to obtain and analyze the physical and chemical properties of those confirmed PNe. In this paper, we present a spectroscopic study of 25 objects reported as potential PNe in catalogs. We derived physical parameters and chemical abundances for some selected objects.

## 2. OBJECT SELECTION

We selected our targets from an exhaustive search in various databases, catalogs, and papers: Acker et al. (1992), Kohoutek (2001), IPHAS (Drew et al. 2005; Viironen et al. 2009; Sabin et al. 2014), MASH (Parker et al. 2006; Miszalski et al. 2008), Ferrero et al. (2015), HASH (Bojić et al. 2017;

Parker et al. 2016), and PNST<sup>4</sup> (Le Dû et al. 2022). Our main selection criterion was objects reported in any catalog as a possible PN, a PN candidate, and confirmed PN with limited or no previous studies.

Table 1 shows all the known, relevant, and updated information found in the literature about our selected sample of 25 objects. It indicates whether spectra, morphologies, central stars, or distances are available. We added their HASH and SIMBAD statuses for comparison.

### 3. OBSERVATIONS AND DATA REDUCTION

Observations were carried out at the Observatorio Astronómico Nacional on the Sierra San Pedro Mártir (hereafter OAN-SPM), and the Observatorio Astrofísico Guillermo Haro (hereafter OAGH). In both cases we used a 2.1 m class telescope. We had three observing runs: 2016 May 7 to 10 (OAGH), 2022 May 24 to 26 and 2022 July 26 to 28 (OAN-SPM). Table 2 shows the observing log, indicating names, coordinates, exposure times, and corresponding observatories. Observations at OAN-SPM were obtained with a seeing of  $3.1''$  on May and  $2.1\text{--}2.3''$  on July, while at OAGH, the seeing was  $1.8\text{--}2.9''$ . At OAN-SPM, low-resolution long-slit spectra were obtained using the Boller & Chivens spectrograph with the SI-2 CCD and a  $400 \text{ lines mm}^{-1}$  dispersion grating, giving a spectral resolution of  $\simeq 6 \text{ \AA}$  (FWHM). In the case of the OAGH, low-resolution long-slit spectra were obtained with the Boller & Chivens spectrograph, the SITe CCD, and a  $150 \text{ lines mm}^{-1}$  dispersion grating resulting in a spectral resolution of  $\simeq 14 \text{ \AA}$  (FWHM). A slit width of  $\simeq 2.6''$  was used in both observatories. The slit was always oriented at a position angle (PA) of  $90^\circ$ , except for PN G006.5+08.7, for which a PA =  $144^\circ$  was used. Appendix A shows the slit positions and extraction zones over-imposed on images of the objects available in HASH. Exposure time for most objects was 1800 s.

For flux calibration, a wider slit width of  $\simeq 13''$  was used to observe the spectrophotometric standard stars BD+28 4211 and Feige 67. Data reduction was carried out following the IRAF standard procedures for bias, flat, wavelength calibration, background, and cosmic ray corrections.

### 4. RESULTS AND DISCUSSION

From our sample of 25 objects we found: 11 objects with clear emission lines, 11 where few emission lines were detected but it was not possible to measure H $\beta$ , and three with no emission lines. Spectra of the 11 objects with clear emission lines are shown in Figure 1. Appendix B shows the spectra for the remaining objects.

---

<sup>4</sup>Planetary Nebula Spectra Trackers (PNST) is a french amateur observational group designed to uncover and confirm new Galactic PNe.

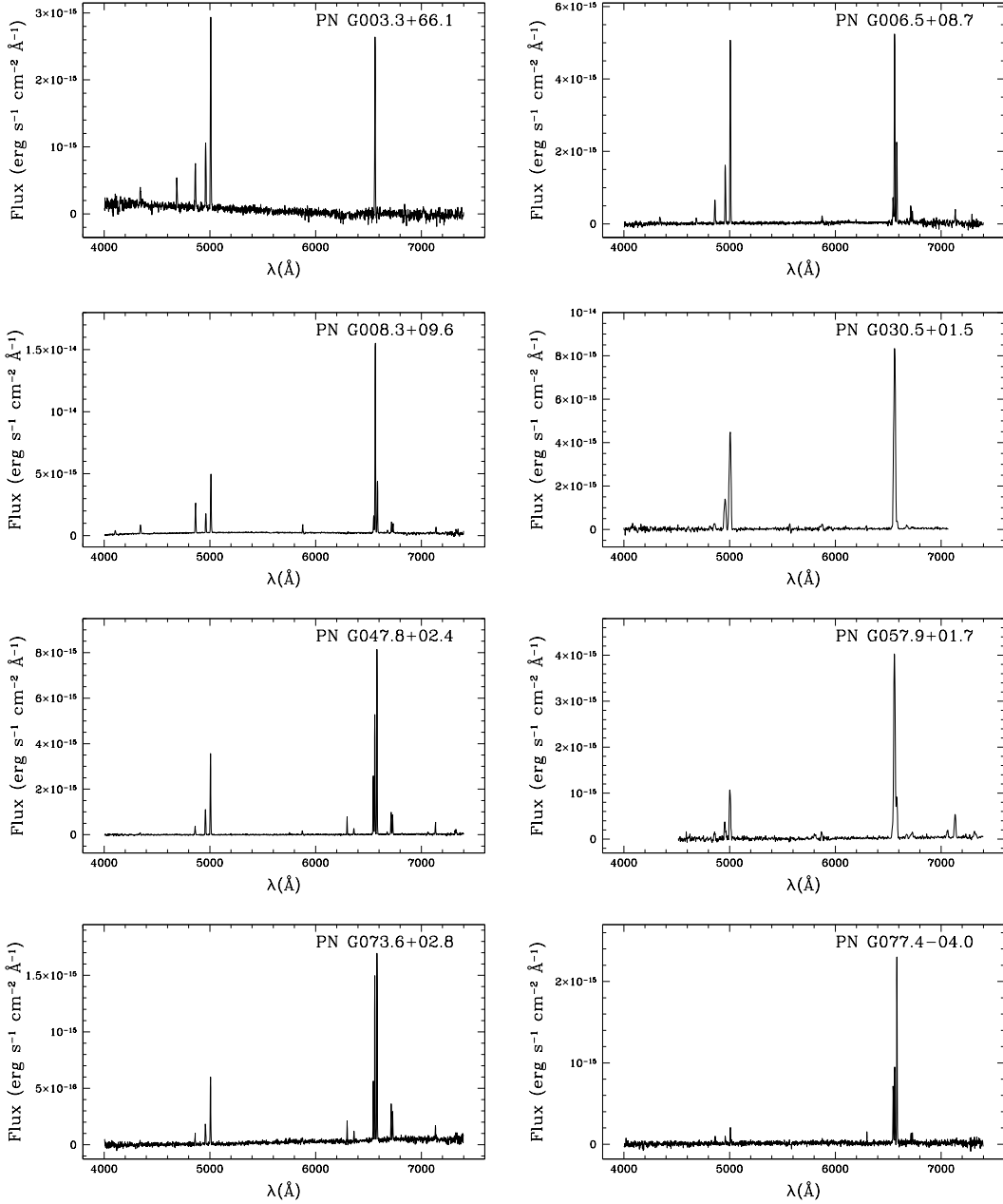


Fig. 1. Spectra for 11 selected objects.

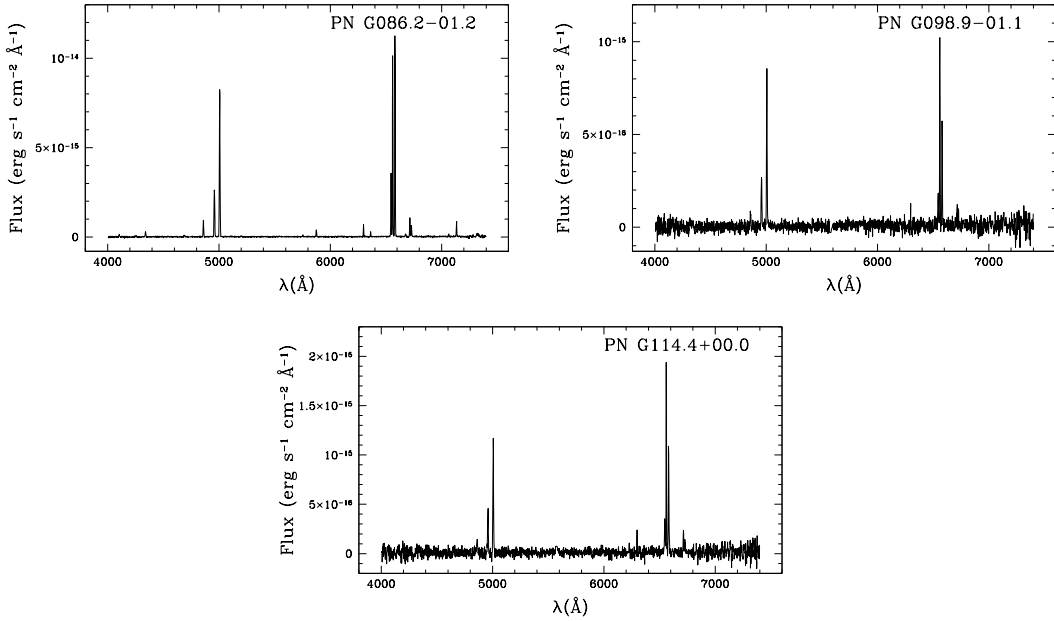


Fig. 1. (Continued).

We used the ANNEB software (Olgún et al. 2011) for line identification, to derive the logarithmic extinction coefficient  $c(\text{H}\beta)$ , to obtain intrinsic line intensities and to calculate physical conditions ( $T_e$  and  $n_e$ ), and ionic and elemental chemical abundances. To obtain ionic abundances, ANNEB uses IRAF's NEBULAR task (Shaw & Dufour 1995) and for deriving elemental abundances uses ionization correction factors from Kingsburgh & Barlow (1994). The uncertainties for all derived quantities were calculated by properly propagating errors in line fluxes, having as a source of error only the number of photons received according the detector gain. Tables 3 and 4 show relative line intensity and derived physical parameters for the 11 objects with multiple emission lines. The extinction function of Cardelli et al. (1989) was adopted to deredden the observed line ratios.  $F(\text{H}\beta)$  corresponds to the observed  $\text{H}\beta$  flux and  $SB(\text{H}\beta)$  to the surface brightness calculated in the extraction area. Three objects show high extinction with  $c(\text{H}\beta) > 2.0$ , which explains the observed weakness in their emission lines.

We present electron temperatures from low-ionization species for two PNe derived using the  $[\text{N II}] (\lambda 6548 + \lambda 6583)/\lambda 5755$  line ratio. The  $[\text{O III}] \lambda 4363$  line was not detected in our sample, preventing the determination of electron temperature using medium-ionization species. Also, we present electron densities from low-ionization species for eight PNe derived using the  $[\text{S II}] \lambda 6716/\lambda 6731$  line ratio. The electron densities in the objects where it could be measured are low, which could indicate that they are possible already evolved PNe. Another possible explanation could be PNe expanding at typical rates but where

the ejected mass was very low, implying low-mass progenitor stars.

Figure 2 show a diagnostic diagram (DD) following Frew & Parker (2010). Eight of our objects are located inside the True PNe region.

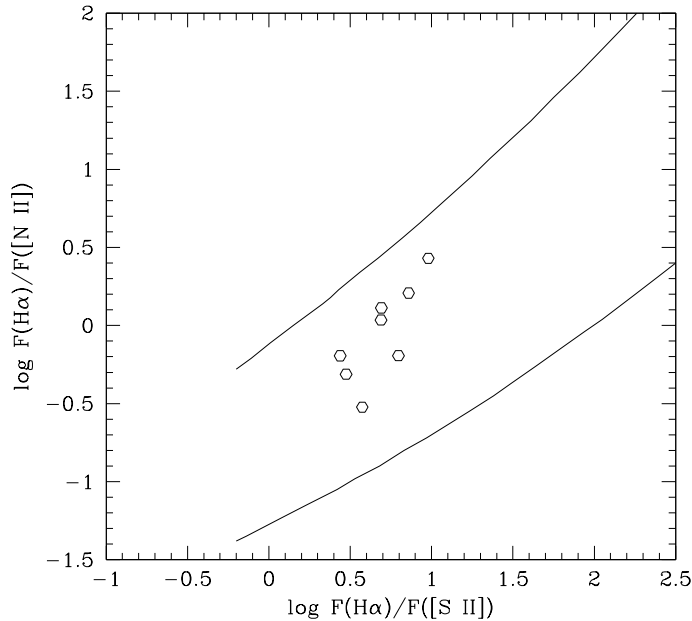


Fig. 2. A  $\log F(\text{H}\alpha)/F([\text{N II}])$  versus  $\log F(\text{H}\alpha)/F([\text{S II}])$  diagnostic diagram.  $F([\text{N II}])$  refers to the sum of the flux of  $\lambda 6548$  and  $\lambda 6583$  nitrogen lines.  $F([\text{S II}])$  refers to the sum of  $\lambda 6716$  and  $\lambda 6731$  sulfur lines. All eight objects lie within the PNe region, as indicated by the empirical boundaries from Frew & Parker (2010). Uncertainties bars are the same size or smaller than the symbols.

Table 5 shows the mean ionic abundances for the 11 selected objects, calculated from the collisionally excited and the optical recombination lines we found. In cases where we could obtain  $T_e$  and  $n_e$ , these values were used in the calculations. Where it was not possible, we adopted  $T_e = 10,000$  K and  $n_e = 100 \text{ cm}^{-3}$ . Table 6 shows elemental abundances in those three objects for which it was possible to derive them. We added some abundance references for the Sun (Asplund et al. 2021), Galactic disk PNe (southern in Kingsburgh & Barlow 1994, northern in Stanghellini et al. 2006) and Galactic bulge PNe (Tan et al. 2024). Values in our data are supersolar, except for O/H and S/H abundances in PN G086.2–01.2 (PN Ra 5) that are sub-solar. Such a low S/H abundance could be explained by the “sulphur anomaly” (Henry et al. 2012). We found congruent elemental abundances with the average values for PNe in our Galaxy. Following classification criteria from Quireza et al. (2007), PN G047.8+02.4 can be classified as a Peimbert type IIa and PN G086.2–01.2 as a Peimbert type I. These results are in agreement with the original criteria used by Peimbert & Torres-Peimbert (1983). Type I PNe are related to massive progenitor stars ( $\sim 2.4\text{--}8.0 M_\odot$ ), while type II are related to less massive

progenitors ( $\sim 1.2\text{--}2.4 M_{\odot}$ , Quireza et al. 2007). Following equations developed by Maciel et al. (2010), we have estimated the central star mass ( $m_{\text{CS}}$ ) and the stellar mass in the main-sequence ( $m_{\text{MS}}$ ) obtaining  $m_{\text{CS}} = 0.6 M_{\odot}$  and  $m_{\text{MS}} = 1.7 M_{\odot}$  for PN G047.8+02.4 and  $m_{\text{CS}} = 0.7 M_{\odot}$  and  $m_{\text{MS}} = 2.3 M_{\odot}$  for PN G086.2–01.2. Following the methodology proposed by Reid & Parker (2010) and using our dereddened line intensity ratios, we could compute the excitation class (EC) based on the presence or absence of He II  $\lambda 4686$  in the nebular spectrum, which defines the EC on a PN. When a PN has  $EC < 5$ , it is considered a low EC; if  $EC \geq 5$ , it is deemed medium to high EC. We found that PN G047.8+02.4 and PN G086.2–01.2 are classified in the medium to high EC with values of 5.7 and 6.9, respectively. In addition, adopting the criterion of  $F([\text{N II}]\lambda 6583)/F(\text{H}\alpha) \geq 1$  as the condition for optically thick PNe (Kaler & Jacoby 1989), PN G047.8+02.4 and PN G086.2–01.2 are optically thick. Therefore, we can use the empirical relationship between  $EC$  and  $T_{\text{eff}}$ , defined by Reid & Parker (2010), to estimate the central star (CS) temperature. In this way, we have found  $T_{\text{eff}} \approx 1.1 \times 10^5$  K for PN G047.8+02.4 and  $T_{\text{eff}} \approx 1.4 \times 10^5$  K for PN G086.2–01.2.

Four low ionization objects were found (PN G047.8+02.4, PN G073.6+02.8, PN G077.4–04.0, and PN G086.2–01.2). For these objects the  $[\text{N II}] \lambda 6583$  line is much more intense than  $\text{H}\alpha$ , especially the case of PN G077.4–04.0 (PN Ra 4) where  $[\text{N II}] \lambda 6583$  is more than twice as intense as  $\text{H}\alpha$ . This phenomenon could be related to shock processes in the nebula as an excitation mechanism (Akras & Gonçalves 2016). To verify this possibility, we have used Raga et al. (2008), Ali & Dopita (2017) and Mari et al. (2023) diagnostic diagrams, as shown in Figure 3. We found that PN G077.4–04.0 is inside a shock region and the excess of the  $[\text{N II}] \lambda 6583$  line could be explained by photoionization and low-velocity shock models. In addition, PN G073.6+02.8 is very close to the contour of the high-speed shock model. This may indicate that a weaker shock is taking place in the nebula.  $[\text{N II}] \lambda 6583$  excess for the remaining two objects could be explained by photoionization models. The central stars of each object in this subgroup must have a low effective temperature.

Table 7 includes 11 objects where measuring a reliable  $\text{H}\beta$  was not possible. However, other emission lines were detected: two objects with several lines and nine with at least evident  $\text{H}\alpha$  emission.  $F(\text{H}\alpha)$  and  $SB(\text{H}\alpha)$  are defined as in Tables 3 and 4 but for  $\text{H}\alpha$ .  $c(\text{H}\beta)_{\text{limit}}$  is the lower limit of  $c(\text{H}\beta)$  derived using an estimation of the upper limit of the  $\text{H}\beta$  flux. This limit was estimated by adding synthetic  $\text{H}\beta$  line profiles of different intensities to our original spectrum and finally choosing a flux where the line was clearly seen in the resulting spectrum. The selected upper limit was typically three times the noise level. We have discarded the four noisiest spectra in the  $c(\text{H}\beta)_{\text{limit}}$  calculations because the detected  $\text{H}\alpha$  had a very low signal to noise (S/N).

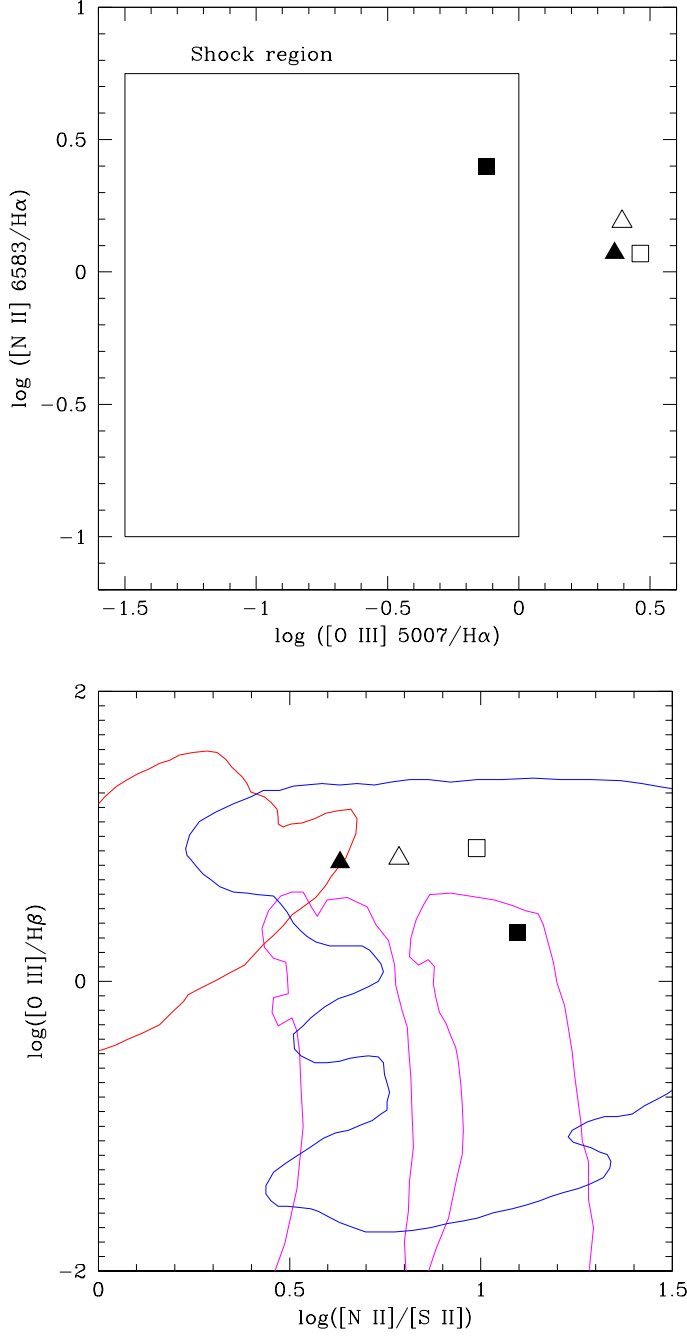


Fig. 3. Diagnostic diagrams to distinguish shock-excited and photoionised regions. Top: proposed by Raga et al. (2008) with the shock region from Ali & Dopita (2017). Bottom: proposed by Mari et al. (2023). Photoionization models are in a blue contour, low-velocity shock models with magenta and high velocity shock models with red. Symbols:  $\triangle$  PN G047.8+02.4,  $\blacktriangle$  PN G073.6+02.8,  $\square$  PN G086.2-01.2, and  $\blacksquare$  PN G077.4-04.0. Uncertainties are the same size or smaller than the symbols.

Table 8 shows angular sizes of the PNe as derived from the H $\alpha$  and [O III]  $\lambda 5007$  emission lines in the 2D long-slit spectra. Only the region with a flux above 1% of the maximum intensity of the line was considered. Some of our values are similar to the major diameters reported by different authors, others are new to the literature. All sizes are affected by seeing at the moment of observation. In addition, in a few cases, the PA of the slit was misaligned with the main axis of the source, which could explain the size differences with values reported in the literature. The most significant difference we found was on PN G003.3+66.1. From our sample, some objects have been observed before by different researchers, as evidenced in Table 1, but no deep studies have appeared in the literature yet. We want to point out that despite the existence of some uploaded spectra in the HASH database, we decided not to use them because presumably are being analyzed by the original authors. Therefore, we have used our spectra in this work. A few objects with spectroscopic or related studies reported in the literature are discussed in the next section. Additional literature information for other objects is available on Appendix C.

## 5. NOTES ON INDIVIDUAL OBJECTS

*PN G008.3+09.6:* Boumis et al. (2006) named this object as PTB 26. These authors reported an optical spectrum where ten emission lines were detected. They derived  $c(\text{H}\beta) = 0.62$  and an electron density  $n_e < 70 \text{ cm}^{-3}$ . We found 14 emission line fluxes,  $c(\text{H}\beta) = 0.96$  and an electron density of  $n_e = 147 \text{ cm}^{-3}$ . Also, we report mean ionic abundances.

*PN G030.5+01.5:* HASH status is True PN, while SIMBAD reports it as an emission-line star based on Robertson & Jordan (1989). In our work, we found the expected characteristics of a PN (see emission lines, abundances and spectrum in the text) but it does not appear on Figure 2, because the [S II] ( $\lambda\lambda 6716, 6731$ ) emission in our spectrum was found not reliable.

*PN G040.1+03.2:* We found probable C IV broad line at 5806 Å. The object has also been observed by Sabin et al. (2014) and the broad emission is clear too. This could be related to a PN with a Wolf-Rayet CS, displaying a blended C IV doublet (at 5801 and 5812 Å) appearing as a broad feature, due to the rapid expansion of the hot stellar wind (DePew et al. 2011).

*PN G041.5+01.7:* Named 1858+0821 by van de Steene et al. (1996). The strength of [N II] $\lambda 6548$  and  $\lambda 6583$  (relative to H $\alpha$ =100) that they reported from a very low S/N spectrum were 24.4 and 66.4, respectively. In our spectrum we only found H $\alpha$  and [N II]  $\lambda 6583$ . The [N II] $\lambda 6548$  line is blended with H $\alpha$ . To correct the H $\alpha$  emission by the  $\lambda 6548$  contribution, we estimated  $\lambda 6548$  using a theoretical ratio  $[\text{N II}]I_{6583}/I_{6548} = 2.96$  (Ueta et al. 2019). The final strengths of the [N II] lines relative to H $\alpha$  are 16 for  $\lambda 6548$  and 47 for  $\lambda 6583$ . Differences found in the ratios can be explained by the very low S/N

of both spectra. Deeper spectrum is needed in order to better understand the nature of this object. However, Urquhart et al. (2009) reported a 6cm radio flux density at 5GHz and associated the source with an object of PN nature.

## 6. CONCLUSIONS

We report a low-resolution spectroscopic investigation of 25 objects suspected to be PNe. Using diagnostic diagrams, we confirmed eight objects as true PNe, while the remaining objects did not exhibit enough emission lines for reliable classification. The true PNe include PN G086.2–01.2 that was previously classified as doubtful and reported as a candidate status in SIMBAD. We have calculated electron temperatures and densities for two and eight PNe respectively, where the S/N in the nebula spectra was appropriate. Ionic abundances are reported for 11 objects and elemental abundances for three objects. Elemental abundances are entirely consistent with Galactic PNe (Kingsburgh & Barlow 1994, Stanghellini et al. 2006 and Tan et al. 2024). We derive masses for the central stars of PN G047.8+02.4 and PN G086.2–01.2 of 0.6 and 0.7  $M_{\odot}$ , respectively. Peimbert types are also reported for these two objects. The large  $[N\,II]\ \lambda 6583/\text{H}\alpha$  line intensity ratio in PN G077.4–04.0 and PN G073.6+02.8 of 2.5 and 1.2, respectively, suggests a contribution of shock excitation, as indicated by shock models. A few emission lines were detected for 11 objects for which we were not able to measure  $\text{H}\beta$ . Deeper spectra are needed to confirm their true nature. We have measured  $\text{H}\alpha$  and  $[\text{O}\,III]\ \lambda 5007$  angular sizes for our sample where possible. Three remaining objects are misclassified as possible PNe, being PN G339.4+29.7 a late-type star, and PN G358.5+09.1 and PN G358.4+08.9 two galaxies.

## 7. ACKNOWLEDGEMENTS

We thank the anonymous referee for providing comments and suggestions that have improved the manuscript. Based upon observations carried out at the Observatorio Astronómico Nacional on the Sierra San Pedro Mártir (OAN-SPM), Baja California, México. We thank the daytime and night support staff at the OAN-SPM for facilitating and helping obtain our observations. This publication is also based on data collected at the Observatorio Astrofísico Guillermo Haro (OAGH), Cananea, México, operated by the Instituto Nacional de Astrofísica, Óptica y Electrónica (INAOE). Funding for the OAGH has been provided by the Consejo Nacional de Humanidades, Ciencias y Tecnologías (CONAHCYT). DABM acknowledges support from CONAHCYT (Mexico) grant 806246. LFM acknowledges support from grants PID2020-114461GB-I00, PID2023-146295NB-I00, and CEX2021-001131-S, funded by MCIN/AEI/10.13039/501100011033. RV acknowledges support from UNAM-DGAPA-PAPIIT grant IN103125. This research used the SIMBAD database, operated at CDS, Strasbourg, France, and the HASH PN database in hashpn.space.

TABLE 1

## LITERATURE INFORMATION OF THE OBSERVED OBJECTS

Name	HASH optical spectra <sup>a</sup>	Morph. <sup>b</sup>	Central Star <sup>c</sup>	$d_{\text{geo}}$ (pc) <sup>d</sup>	$d_{\text{phot}}$ (pc) <sup>d</sup>	HASH <sup>e</sup>	SIMBAD <sup>f</sup>
PN G003.3+66.1	...	R	1227151802340968832	729 <sup>+176</sup> <sub>-126</sub>	464 <sup>+32</sup> <sub>-18</sub>	P	PN
PN G339.4+29.7	...	...	...	...	...	NPN	PNC
PN G358.5+09.1	...	...	...	...	...	PG	PNC
PN G358.4+08.9	...	...	...	...	...	PG	PNC
PN G006.5+08.7	...	Ea*	4122534632633972992	3327 <sup>+853</sup> <sub>-602</sub>	3374 <sup>+2278</sup> <sub>-1058</sub>	T	PN
PN G008.3+09.6	SO, 2002, 0.3m, 1×3600s	B*	4124562102059801216	8402 <sup>+2263</sup> <sub>-1735</sub>	7996 <sup>+1518</sup> <sub>-1495</sub>	T	PN
PN G031.3+02.0	...	S	...	...	...	P	S
PN G030.5+01.5	SSO, 2008, 2.3m, 1×300s	E	4260148618930827008	...	...	T	ELS
PN G040.1+03.2	SAAO, 2011, 1.9m, 1×1200s	Eam†	4310230750781889920	7961 <sup>+3458</sup> <sub>-3893</sub>	4786 <sup>+1331</sup> <sub>-1662</sub>	T	PN
PN G038.4+02.2	KPNO, 2009, 2.1m, 1×1800s	R†	...	...	...	T	PN
PN G040.6+01.5	SAAO, 2011, 1.9m, 1×1200s	B/S‡	...	...	...	T	PN
PN G041.5+01.7	KPNO, 1993, 2.1m, 1×900s	S†	4310136536377607040	...	...	L	PN
PN G047.8+02.4	KPNO, 2009, 2.1m, 1×1800s	E†	...	...	...	T	PN
PN G050.0+01.0	...	E	4320871725541398400	...	...	T	PNC
PN G051.8+01.7	...	S	4514907211117285504	...	...	P	S
PN G052.0+01.7	...	E	...	...	...	L	MIRS
PN G051.7+01.3	OAN-SPM, 2010, 2.1m, 1×1800s	Ia†	4322743914667694208	...	...	T	PN
PN G057.9+01.7	...	R	2019455895594998784	5556 <sup>+10,502</sup> <sub>-2409</sub>	6174 <sup>+2448</sup> <sub>-2826</sub>	T	PNC
PN G058.6+00.9	...	S	2020219403339189760	...	...	P	PN
PN G073.6+02.8	KPNO, 2009, 2.1m, 1×1800s	East†	...	...	...	T	PN
PN G077.4–04.0	...	Es‡	...	...	...	T	PN
PN G086.2–01.2	...	B	...	...	...	T	PNC
PN G095.8+02.6	GTC, 2011, 10.4m, 1×2400s	Eps†	...	...	...	T	PN
PN G098.9–01.1	OAN-SPM, 2011, 2.1m, 1×1800s	Ra†	1981477771828655488	5583 <sup>+2964</sup> <sub>-2607</sub>	5501 <sup>+1486</sup> <sub>-808</sub>	T	PN
PN G114.4+00.0	...	E‡	2012536875076571776	3367 <sup>+2219</sup> <sub>-1197</sub>	4251 <sup>+1219</sup> <sub>-920</sub>	T	PN

<sup>a</sup> Observatory, date, telescope diameter, and exposure time. Spectra that are not flux-calibrated were not included.<sup>b</sup>Morphology. Round (R), elliptical (E), bipolar (B), star-like (S), irregular (I), sided asymmetry (a), multiple shells (m), internal structure (s), and point symmetry (p). \*Parker et al. (2006), †Sabin et al. (2014), and ‡Sabin et al. (2021). Morphologies without references assigned by HASH.<sup>c</sup>DR3 IDs (Gaia Collaboration et al. 2023) according to Chornay & Walton (2021), and González-Santamaría et al. (2021).<sup>d</sup>Geometric distance ( $d_{\text{geo}}$ ) and photogeometric distance ( $d_{\text{phot}}$ ) calculated by Bailer-Jones et al. (2021).<sup>e</sup>HASH status. For Planetary Nebula (PN): Possible (P), True (T), and Likely (L). Other objects: Not PN (NPN) and Possible galaxy (PG).<sup>f</sup>SIMBAD status. PN Candidate (PNC), Star (S), Emission-line Star (ELS), and MIRS (Mid-IR Source).

TABLE 2  
OBSERVED OBJECTS

Name	RA (2000)	DEC (2000)	$t_{\text{exp}}$ (s)	OBSERVAT	DATE
PN G003.3+66.1	14:16:21.95	+13:52:24.25	3×1800	OAN-SPM	2022 May 24
PN G339.4+29.7	15:08:20.73	-23:14:50.47	1×1800	OAN-SPM	2022 May 24
PN G358.5+09.1	17:07:45.52	-25:03:38.87	1×1800	OAN-SPM	2022 July 27
PN G358.4+08.9	17:08:19.73	-25:13:41.60	1×1800	OAN-SPM	2022 July 26
PN G006.5+08.7 <sup>a</sup>	17:28:14.05	-18:44:31.01	3×1800	OAN-SPM	2022 May 24
PN G008.3+09.6	17:29:13.10	-16:47:42.60	3×1800	OAN-SPM	2022 May 24
PN G031.3+02.0	18:41:25.95	-00:27:45.41	1×1200	OAGH	2016 May 07
PN G030.5+01.5	18:41:40.43	-01:25:17.72	1×1800	OAGH	2016 May 07
PN G040.1+03.2	18:53:09.40	+07:52:41.00	3×1800	OAGH	2016 May 08
PN G038.4+02.2	18:53:21.74	+05:56:42.12	1×1800	OAGH	2016 May 08
PN G040.6+01.5	18:59:57.00	+07:35:44.00	1×1800	OAGH	2016 May 10
PN G041.5+01.7	19:01:05.72	+08:25:35.93	1×1200	OAGH	2016 May 08
PN G047.8+02.4	19:10:01.10	+14:22:02.00	1×1800	OAN-SPM	2022 July 28
PN G050.0+01.0	19:19:22.92	+15:41:37.15	1×1800	OAGH	2016 May 09
PN G051.8+01.7	19:20:31.62	+17:32:48.92	1×1800	OAGH	2016 May 09
PN G052.0+01.7	19:20:54.53	+17:46:07.90	1×1800	OAGH	2016 May 09
PN G051.7+01.3	19:21:46.61	+17:20:45.80	1×1800	OAN-SPM	2022 July 26
PN G057.9+01.7	19:33:09.03	+22:58:33.63	1×1800	OAGH	2016 May 10
PN G058.6+00.9	19:37:29.33	+23:09:46.56	1×1800	OAGH	2016 May 10
PN G073.6+02.8	20:05:22.00	+36:59:42.00	1×1800	OAN-SPM	2022 July 28
PN G077.4-04.0	20:44:14.10	+36:07:37.00	1×1800	OAN-SPM	2022 July 28
PN G086.2-01.2	21:02:38.73	+44:46:46.00	1×1800	OAN-SPM	2022 July 28
PN G095.8+02.6	21:26:08.30	+54:20:15.00	1×1800	OAN-SPM	2022 July 26
PN G098.9-01.1	21:58:42.30	+53:30:03.00	1×1800	OAN-SPM	2022 July 26
PN G114.4+00.0	23:38:40.43	+61:41:40.90	1×1800	OAN-SPM	2022 July 26

<sup>a</sup>Only object observed with PA = 144°.

TABLE 3  
INTRINSIC LINE INTENSITIES ( $I(H\beta) = 100$ ) AND PHYSICAL PARAMETERS FOR THE FIRST SET OF OBJECTS

Ion	Line	$f_\lambda$	003.3+66.1	006.5+08.7	008.3+09.6	030.5+01.5	047.8+02.4	057.9+01.7
H $\delta$	4101	0.230	8 ± 1	...	27 ± 1	...	...	...
H $\gamma$	4340	0.157	48 ± 1	52 ± 1	48 ± 1	...	51 ± 2	...
He I	4471	0.115	...	6 ± 1	6 ± 1	...	...	...
He II	4686	0.050	55 ± 1	30 ± 1	...	...	6 ± 1	...
H $\beta$	4861	0.000	100 ± 1	100 ± 1	100 ± 1	100 ± 1	100 ± 2	100 ± 1
[O III]	4959	-0.026	141 ± 2	236 ± 2	58 ± 1	409 ± 2	243 ± 4	165 ± 1
[O III]	5007	-0.038	366 ± 3	662 ± 6	172 ± 1	1169 ± 4	707 ± 10	471 ± 4
[N II]	5755	-0.185	...	...	...	...	6 ± 1	...
He I	5876	-0.203	...	12 ± 1	15 ± 1	20 ± 1	14 ± 1	17 ± 1
[O I]	6300	-0.263	...	...	...	...	48 ± 1	...
[O I]	6363	-0.271	...	...	...	...	17 ± 1	...
[N II]	6548	-0.296	...	...	...	...	143 ± 3	...
Ha	6563	-0.298	286 ± 4	287 ± 4	286 ± 2	286 ± 2	286 ± 6	286 ± 3
[N II]	6583	-0.300	...	130 ± 2	79 ± 1	5 ± 1	443 ± 9	47 ± 1
He I	6678	-0.313	...	48 ± 1	28 ± 1	...	5 ± 1	5 ± 1
[S II]	6716	-0.318	...	130 ± 2	79 ± 1	5 ± 1	51 ± 1	9 ± 1 <sup>a</sup>
[S II]	6731	-0.320	...	5 ± 1	4 ± 1	...	46 ± 1	...
He I	7065	-0.364	...	...	...	...	5 ± 1	7 ± 1
[Ar III]	7136	-0.374	...	15 ± 1	7 ± 1	...	22 ± 1	19 ± 1
[O II]	7320	-0.398	...	...	...	...	5 ± 1	5 ± 1 <sup>b</sup>
[O II]	7330	-0.400	...	...	...	...	12 ± 1	...
$\log F(H\beta)$	—	—	-14.19 ± 0.01	-14.26 ± 0.01	-13.70 ± 0.01	-14.22 ± 0.01	-14.50 ± 0.01	-14.58 ± 0.01
$SB(H\beta)^c$	—	—	2.75	4.62	19.40	26.37	9.05	15.73
$c(H\beta)$	—	—	0.09 ± 0.01	1.26 ± 0.01	0.96 ± 0.01	3.33 ± 0.01	1.83 ± 0.02	3.29 ± 0.01
$T_e(\text{[N II]})$	—	—	...	...	...	...	10,295 ± 258	...
$n_e(\text{[S II]})$	—	—	...	< 100	147 ± 33	...	381 ± 90	...

<sup>a</sup>Correspond to  $\lambda 6716$  and  $\lambda 6731$  sulfur lines blended.

<sup>b</sup>Correspond to  $\lambda 7320$  and  $\lambda 7330$  oxygen lines blended.

<sup>c</sup>Surface brightness ( $\times 10^{-17} \text{ erg s}^{-1} \text{ cm}^{-2} \text{ arcsec}^{-2}$ ).

TABLE 4  
INTRINSIC LINE INTENSITIES ( $I(H\beta) = 100$ ) AND PHYSICAL PARAMETERS FOR THE SECOND SET OF OBJECTS

Ion	Line	$f_\lambda$	073.6+02.8	077.4-04.0	086.2-01.2	098.9-01.1	114.4+00.0
H $\delta$	4101	0.230	84 ± 6	...	34 ± 1	...	...
H $\gamma$	4340	0.157	...	...	66 ± 1	...	...
He I	4471	0.115	...	...	...	...	...
He II	4686	0.050	...	...	19 ± 1	...	...
H $\beta$	4861	0.000	100 ± 5	100 ± 4	100 ± 1	100 ± 4	100 ± 3
[O III]	4959	-0.026	230 ± 9	66 ± 3	278 ± 3	276 ± 9	193 ± 4
[O III]	5007	-0.038	663 ± 23	216 ± 8	830 ± 8	851 ± 26	535 ± 11
[N II]	5755	-0.185	...	...	6 ± 1	...	...
He I	5876	-0.203	22 ± 1	23 ± 1	17 ± 1	...	...
[O I]	6300	-0.263	42 ± 2	34 ± 2	22 ± 1	65 ± 2	88 ± 3
[O I]	6363	-0.271	19 ± 1	7 ± 1	8 ± 1	...	...
[N II]	6548	-0.296	110 ± 5	241 ± 11	109 ± 2	60 ± 3	66 ± 2
H $\alpha$	6563	-0.298	286 ± 14	286 ± 13	285 ± 4	287 ± 13	286 ± 8
[N II]	6583	-0.300	337 ± 16	714 ± 32	336 ± 5	161 ± 7	198 ± 6
He I	6678	-0.313	...	...	5 ± 1	...	...
[S II]	6716	-0.318	57 ± 3	43 ± 2	27 ± 1	43 ± 2	33 ± 1
[S II]	6731	-0.320	47 ± 3	34 ± 2	19 ± 1	16 ± 1	26 ± 1
He I	7065	-0.364	...	...	4 ± 1	...	...
[Ar III]	7136	-0.374	16 ± 1	...	19 ± 1	...	...
[O II]	7320	-0.398	...	...	4 ± 1	...	...
[O II]	7330	-0.400	...	...	4 ± 1	...	...
$\log F(H\beta)$	—	—	-15.29 ± 0.01	-15.24 ± 0.01	-14.18 ± 0.01	-15.20 ± 0.01	-14.83 ± 0.01
$SB(H\beta)^a$	—	—	1.44	0.92	10.87	0.03	1.11
$c(H\beta)$	—	—	2.53 ± 0.05	1.78 ± 0.05	1.61 ± 0.01	1.75 ± 0.04	1.26 ± 0.03
$T_e([N II])$	—	—	...	...	11,445 ± 216	...	...
$n_e([S II])$	—	—	230 ± 170	175 ± 163	< 100	< 100	155 ± 111

<sup>a</sup>Surface brightness ( $\times 10^{-17} \text{ erg s}^{-1} \text{ cm}^{-2} \text{ arcsec}^{-2}$ ).

TABLE 5

MEAN IONIC ABUNDANCES<sup>a</sup> FROM ALL THE SELECTED OBJECTS

Ion	Factor	003.3+66.1	006.5+08.7	008.3+09.6	030.5+01.5	047.8+02.4	057.9+01.7
He <sup>1+</sup>	$\times 10^{-1}$	...	1.09 ± 0.02	1.08 ± 0.01	1.55 ± 0.01	1.17 ± 0.02	1.28 ± 0.01
He <sup>2+</sup>	$\times 10^{-2}$	4.48 ± 0.06	2.40 ± 0.04	...	...	0.47 ± 0.03	...
N <sup>1+</sup>	$\times 10^{-5}$	...	2.65 ± 0.03	1.56 ± 0.01	0.09 ± 0.01	7.94 ± 0.47	0.92 ± 0.01
O <sup>0+</sup>	$\times 10^{-4}$	...	...	...	...	0.86 ± 0.07	...
O <sup>1+</sup>	$\times 10^{-4}$	...	...	...	...	2.57 ± 0.50	1.95 ± 0.03
O <sup>2+</sup>	$\times 10^{-4}$	1.36 ± 0.01	2.39 ± 0.01	0.60 ± 0.01	4.18 ± 0.01	2.26 ± 0.16	1.69 ± 0.01
S <sup>1+</sup>	$\times 10^{-6}$	...	0.89 ± 0.01	0.69 ± 0.01	...	2.19 ± 0.17	0.34 ± 0.01
Ar <sup>2+</sup>	$\times 10^{-6}$	...	1.41 ± 0.03	0.62 ± 0.01	...	1.91 ± 0.16	1.76 ± 0.02

Ion	Factor	073.6+02.8	077.4-04.0	086.2-01.2	098.9-01.1	114.4+00.0
He <sup>1+</sup>	$\times 10^{-1}$	1.58 ± 0.08	1.71 ± 0.09	1.32 ± 0.02	...	...
He <sup>2+</sup>	$\times 10^{-2}$	...	...	1.56 ± 0.04	...	...
N <sup>1+</sup>	$\times 10^{-5}$	6.52 ± 0.23	14.01 ± 0.49	4.65 ± 0.19	3.31 ± 0.11	3.86 ± 0.09
O <sup>0+</sup>	$\times 10^{-4}$	0.94 ± 0.03	0.59 ± 0.02	0.27 ± 0.02	1.26 ± 0.05	1.69 ± 0.05
O <sup>1+</sup>	$\times 10^{-4}$	...	...	0.81 ± 0.08	...	...
O <sup>2+</sup>	$\times 10^{-4}$	2.35 ± 0.07	0.74 ± 0.02	1.88 ± 0.09	2.97 ± 0.07	1.93 ± 0.03
S <sup>1+</sup>	$\times 10^{-6}$	2.47 ± 0.19	1.79 ± 0.14	0.75 ± 0.03	1.34 ± 0.05	1.37 ± 0.08
Ar <sup>2+</sup>	$\times 10^{-6}$	1.47 ± 0.09	...	1.29 ± 0.08	...	...

<sup>a</sup> Given as  $N(X^{i+})/N(H^+)$ .

TABLE 6

ELEMENTAL ABUNDANCES<sup>a</sup> FROM SOME SELECTED OBJECTS

Ion	Factor	006.5+08.7	047.8+02.4	086.2-01.2	Sun <sup>b</sup>	KB94 <sup>c</sup>	SGC06 <sup>c</sup>	TPZ24 <sup>c</sup>
He	1	0.133 ± 0.002	0.122 ± 0.003	0.147 ± 0.002	0.082	0.115 (55)	0.123 (75)	0.115 (123)
N	$\times 10^{-4}$	...	1.532 ± 0.357	1.660 ± 0.193	0.676	2.239 (47)	2.439 (63)	1.862 (122)
O	$\times 10^{-4}$	...	4.964 ± 0.548	2.904 ± 0.134	4.898	4.786 (54)	3.531 (67)	5.012 (124)
S	$\times 10^{-5}$	...	1.511 ± 0.124	0.626 ± 0.041	1.318	0.832 (43)	...	0.794 (124)
Ar	$\times 10^{-6}$	2.648 ± 0.583	3.574 ± 0.840	2.420 ± 0.550	2.399	2.455 (41)	1.262 (46)	2.754 (122)

<sup>a</sup> Given as  $N(X)/N(H)$ .<sup>b</sup> According to Asplund et al. (2021).<sup>c</sup> Average PNe abundances. KB94 is for Kingsburgh & Barlow (1994), SGC06 for Stanghellini et al. (2006), and TPZ24 for Tan et al. (2024). The number of PNe used for each average appear in parentheses.

TABLE 7  
OBJECTS WITH FEW EMISSION LINES DETECTED

Ion	Line	031.3+02.0	040.1+03.2 <sup>a</sup>	038.4+02.2	040.6+01.5	041.5+01.7	050.0+01.0
[O III]	4959	...	13 ± 1	...	...	...	...
[O III]	5007	...	30 ± 1	19 ± 1	...	...	24 ± 1
[N II]	6548	...	...	...	...	...	...
H $\alpha$	6563	100 ± 1	100 ± 1	100 ± 1	100 ± 1	100 ± 1 <sup>b</sup>	100 ± 1
[N II]	6583	...	4 ± 1	...	...	40 ± 1	...
[S II]	6716	...	...	...	...	...	...
[S II]	6731	...	...	...	...	...	...
[Ar III]	7136	...	...	...	...	...	...
$\log F(\text{H}\alpha)$	—	-14.29 ± 0.01	-13.31 ± 0.01	-13.80 ± 0.01	-14.89 ± 0.01	-14.19 ± 0.01	-14.11 ± 0.01
$SB(\text{H}\alpha)^c$	—	6.16	16.78	11.01	1.33	10.71	10.73
$c(\text{H}\beta)_{\text{limit}}$	—	> 0.81	> 3.04	> 1.82	...	...	> 1.67
<hr/>							
Ion	Line	051.8+01.7	052.0+01.7	051.7+01.3	058.6+00.9	095.8+02.6	
[O III]	4959	...	...	15 ± 1	...	...	12 ± 1
[O III]	5007	...	...	43 ± 1	...	...	39 ± 1
[N II]	6548	...	...	29 ± 1	...	...	33 ± 1
H $\alpha$	6563	100 ± 1	100 ± 1	100 ± 2	100 ± 3	100 ± 1	110 ± 2
[N II]	6583	...	...	97 ± 2	...	...	12 ± 1
[S II]	6716	...	...	16 ± 1	...	...	8 ± 1
[S II]	6731	...	...	12 ± 1	...	...	14 ± 1
[Ar III]	7136	...	...	23 ± 1	...	...	
$\log F(\text{H}\alpha)$	—	-14.82 ± 0.01	-13.72 ± 0.01	-14.42 ± 0.01	-15.40 ± 0.01	-14.19 ± 0.01	
$SB(\text{H}\alpha)^a$	—	2.11	13.12	0.53	0.66	1.60	
$c(\text{H}\beta)_{\text{limit}}$	—	...	> 1.08	> 2.31	...	> 3.16	
<hr/>							

<sup>a</sup>We found also I(C IV) = 16 ± 1, see § 5.

<sup>b</sup>Blended with  $\lambda$ 6548, see § 5.

<sup>c</sup>Surface brightness ( $\times 10^{-16}$  erg s<sup>-1</sup> cm<sup>-2</sup> arcsec<sup>-2</sup>).

<sup>a</sup>Surface brightness ( $\times 10^{-16}$  erg s<sup>-1</sup> cm<sup>-2</sup> arcsec<sup>-2</sup>).

TABLE 8  
OBJECT SIZES<sup>a</sup> FROM OUR SAMPLE

Name	[O III]	5007 (arcsec)	H $\alpha$ 6563 (arcsec)	Literature major diameter (arcsec)
PN G003.3+66.1	106	100	50 (Frew et al. 2016)	
PN G339.4+29.7	...	...	...	...
PN G358.5+09.1	...	...	...	...
PN G358.4+08.9	...	...	...	...
PN G006.5+08.7	47	45	51 (Parker et al. 2006)	
PN G008.3+09.6	29	38	30 (Parker et al. 2006)	
PN G031.3+02.0	...	3	...	
PN G030.5+01.5	8	11	...	...
PN G040.1+03.2	5	7	12 (Sabin et al. 2014)	
PN G038.4+02.2	4	4	5 Sabin et al. (2014)	
PN G040.6+01.5	...	3	5 (Sabin et al. 2021)	
PN G041.5+01.7	...	3	...	
PN G047.8+02.4	10	12	10 (Sabin et al. 2014)	
PN G050.0+01.0	3	3	...	
PN G051.8+01.7	...	3	...	
PN G052.0+01.7	...	5	...	
PN G051.7+01.3	23	25	34 (Sabin et al. 2021)	
PN G057.9+01.7	5	6	...	
PN G058.6+00.9	...	3	...	
PN G073.6+02.8	10	12	11 (Sabin et al. 2014)	
PN G077.4-04.0	14	23	25 (Sabin et al. 2021)	
PN G086.2-01.2	15	17	12 Ferrero et al. (2015)	
PN G095.8+02.6	9	12	15 (Sabin et al. 2021)	
PN G098.9-01.1	26	26	31 (Sabin et al. 2021)	
PN G114.4+00.0	55	56	61 (Sabin et al. 2021)	

<sup>a</sup>Uncertainties are determined by the seeing, with a typical value of 2 arcsec.

## APPENDICES

## APPENDIX A: SLIT POSITION AND SPECTRUM EXTRACTION ZONE

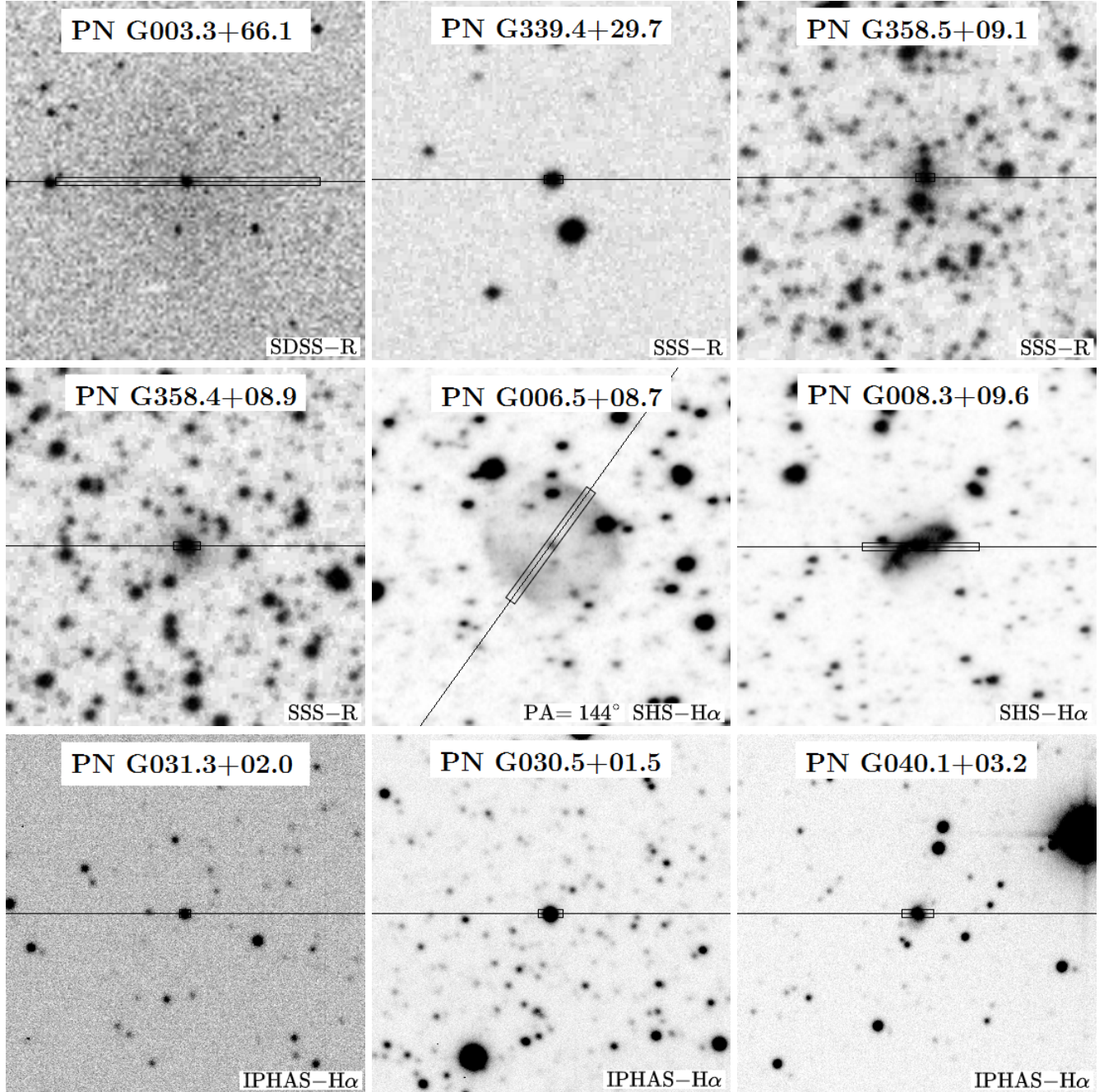


Fig. A1. Visual fields available in HASH for observed objects with images taken from SDSS (York et al. 2000), SSS (Hambly et al. 2001), SHS (Parker et al. 2005), and IPHAS (Drew et al. 2005), as labeled in the bottom right corner of each panel. North is up, East is left. Field size is  $2' \times 2'$  in all cases. Solid line represents the long-slit position which was oriented at PA =  $90^\circ$  for all objects except where indicated. The rectangle over the long-slit marks the extraction zone for the spectra shown in Figure 1 and Appendix B.

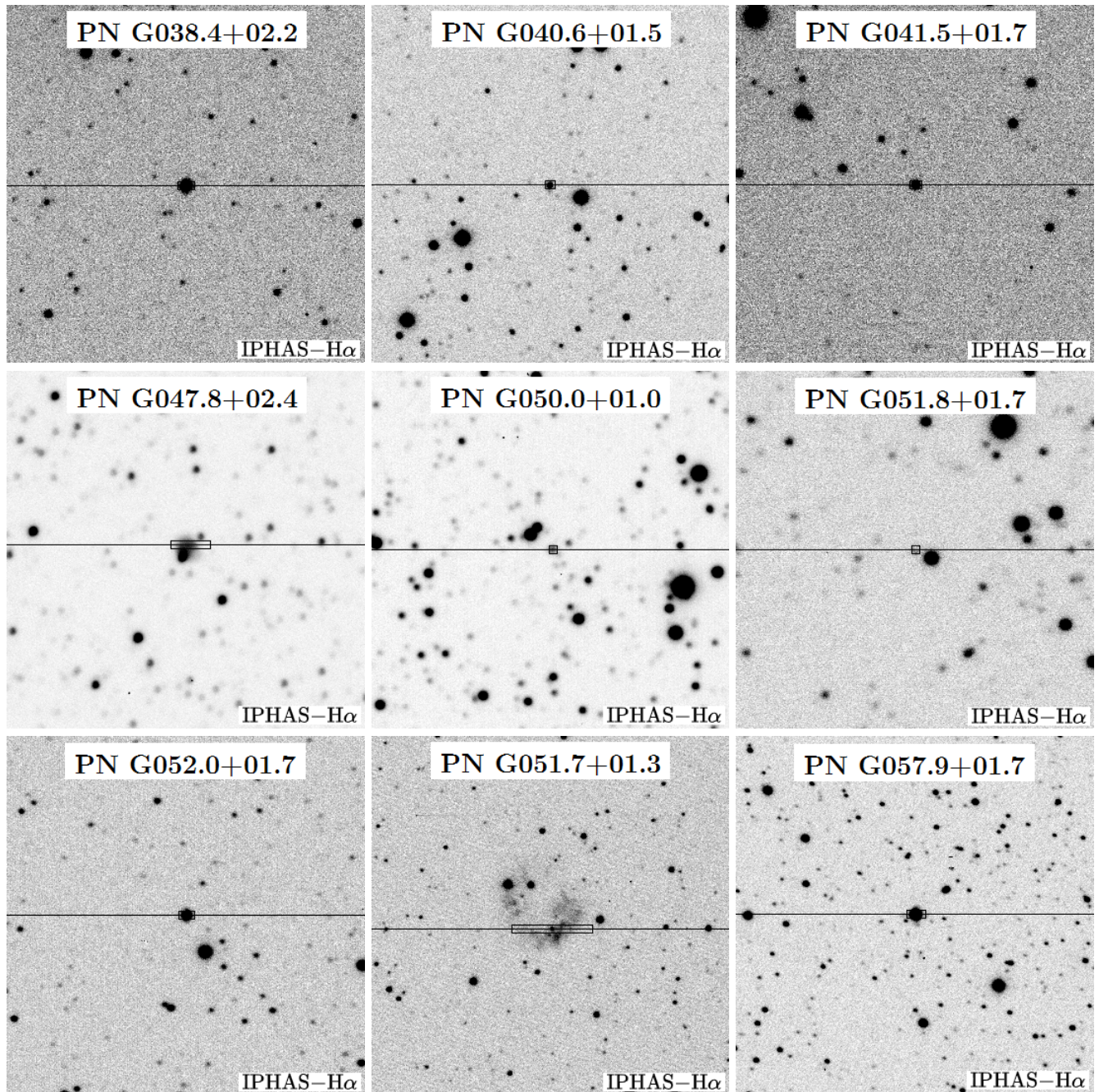


Fig. A1. (Continued).

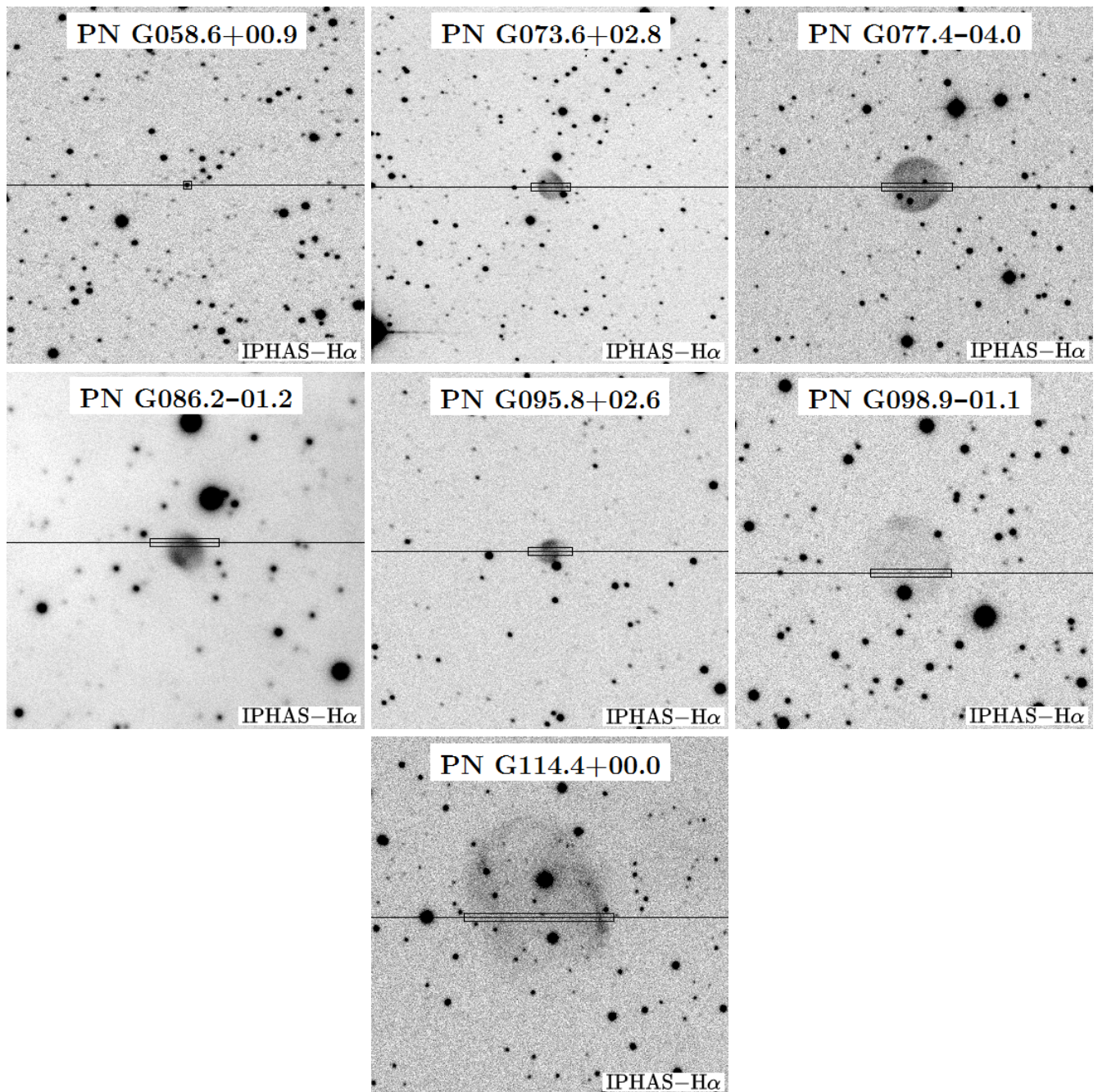


Fig. A1. (Continued).

## APPENDIX B: SPECTRA OF THE REMAINING 14 OBJECTS

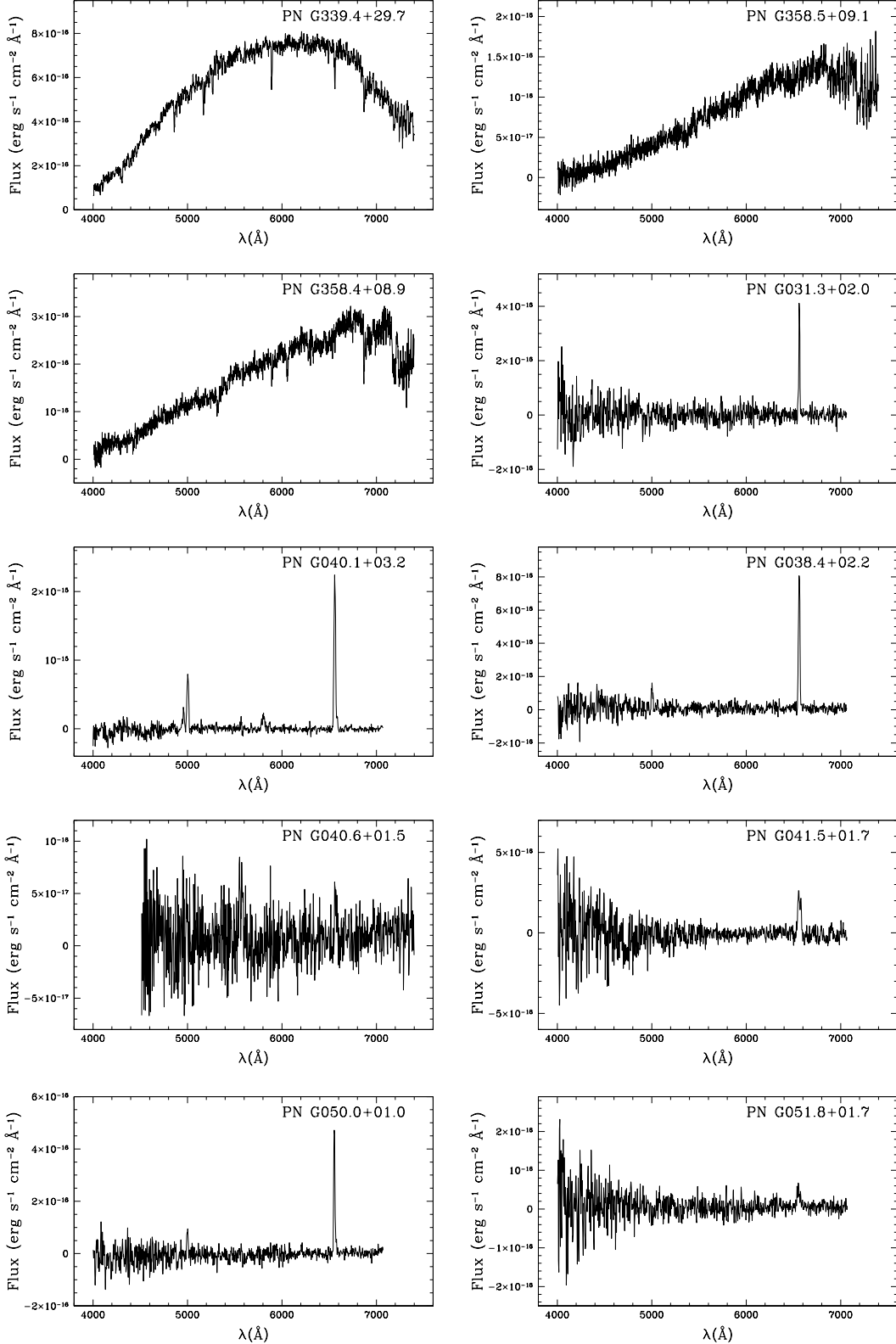


Fig. A2. Spectra of 14 objects with a few or no emission lines.

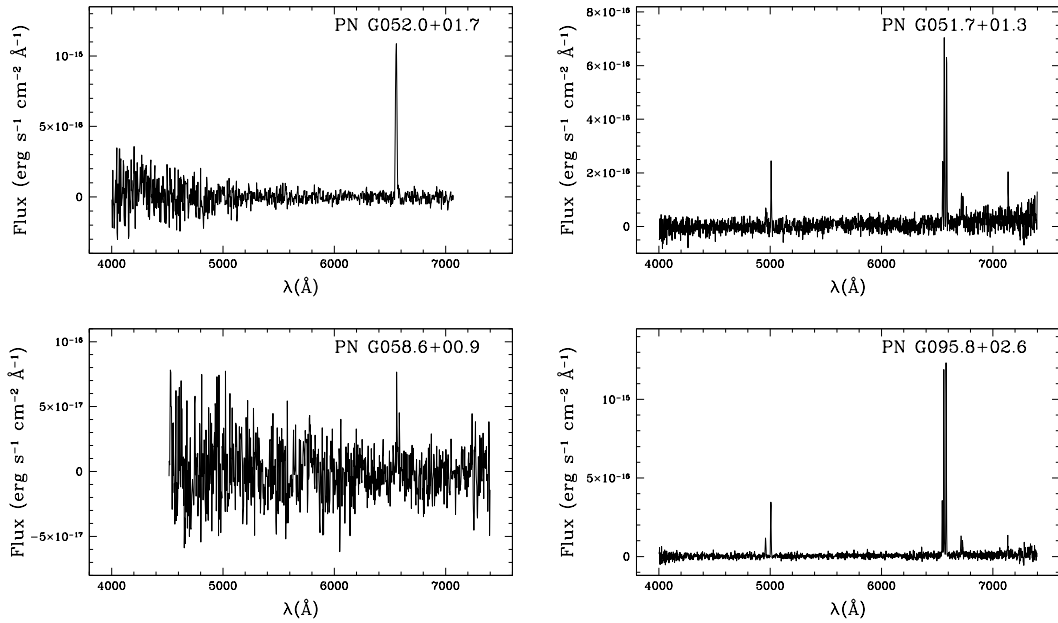


Fig. A2. (Continued).

## APPENDIX C: ADDITIONAL LITERATURE INFORMATION

There are different collective works in the literature that involve some of the objects in our sample with topics that are not related to our research. The objects and papers where they appear are listed in Table A1.

TABLE A1  
COLLECTIVE WORKS<sup>a</sup> THAT INCLUDES OBJECTS IN OUR SAMPLE

Name	1	2	3	4	5	6	7	8	9	10	11
PN G003.3+66.1	...	...	...	✓	...	✓	...	...	...	✓	✓
PN G006.5+08.7	...	...	...	✓	...	...	...	...	✓	...	✓
PN G008.3+09.6	...	...	✓	...	...	...	...	...	✓	...	✓
PN G031.3+02.0	...	...	...	...	...	...	...	...	...	...	✓
PN G030.5+01.5	...	...	...	...	...	...	...	...	...	...	✓
PN G040.1+03.2	...	...	...	...	...	...	...	...	...	✓	✓
PN G038.4+02.2	...	...	...	...	...	...	...	...	...	✓	...
PN G040.6+01.5	...	...	...	...	...	...	...	...	...	✓	...
PN G041.5+01.7	✓	...	...	...	...	...	...	...	...	✓	...
PN G047.8+02.4	...	...	...	...	...	...	...	...	...	...	✓
PN G050.0+01.0	...	...	...	...	...	...	...	✓	...	...	✓
PN G052.0+01.7	✓	...	...	...	...	...	...	...	...	...	✓
PN G051.7+01.3	...	...	...	...	✓	...	...	...	✓	...	...
PN G057.9+01.7	✓	✓	...	...	...	...	...	...	...	✓	✓
PN G058.6+00.9	✓	...	...	...	...	...	...	✓	...	...	✓
PN G073.6+02.8	...	...	...	...	...	...	...	...	...	...	✓
PN G077.4-04.0	...	...	...	...	...	...	...	...	...	...	✓
PN G086.2-01.2	...	...	...	...	...	...	...	...	...	...	✓
PN G095.8+02.6	...	...	...	...	...	...	✓	...	...	...	...
PN G114.4+00.0	...	...	...	...	...	...	...	...	...	...	✓

<sup>a</sup>1 (Condon et al. 1999) and 3 (Bojić et al. 2011) reported flux density at 1.4 GHz. 2 Stanghellini et al. (2008) and 6 (Frew et al. 2016) created a catalog of statistical distances. 4 (Frew et al. 2013) made a catalog of integrated H $\alpha$  fluxes. 5 (Froebrich et al. 2015) have identified extended H $_2$  features. 7 (Ramos-Larios et al. 2017) found that the spatial distribution of H $_2$  confirms its bipolar morphology. 8 (Irabor et al. 2018) reported flux at 5 GHz and brightness temperature. 9 (Jacoby et al. 2021) reported a study of the possible light curve variability on their CSs. 10 (Hajduk et al. 2021) made radio observations to find evidence of cold plasma component coexisting with hot plasma, but the objects were undetected by the experiment. 11 (Gómez-Muñoz et al. 2023) created an UV and optical catalog.

Some individual notes for other objects are:

*PN G003.3+66.1 (SkAc 1):* Its central star is very well studied by several authors, such as Kepler et al. (2016) showing the spectra of the white dwarf, Weidmann et al. (2020) indicating its spectral classification and Gentile Fusillo et al. (2021) listing stellar properties. Also, Douchin et al. (2015) present an image using [O III]  $\lambda 5007$  filter. Although it does not appear in the diagnostic diagram we presented in Figure 2, Makarov et al. (2003) classified this object as probable PN due to its low heliocentric radial velocity ( $-17 \pm 2 \text{ km s}^{-1}$ ).

*PN G339.4+29.7 (PN Y-C 2-17):* This object was discovered originally by Cesco & Gibson (1973) and it was described as a PN using only morphological features on a photographic plate; eventually, was cataloged as a Possible PN in Kohoutek (2001) and no other studies have been conducted to date. HASH status is Not PN, while SIMBAD status is PN candidate. We have not found any emission lines in our spectrum but we have identified the object as an evolved star of spectral type K3I-II.

*PN G358.5+09.1 (Terz N 26, LEDA 89007):* Discovered by Terzan (1985) who described it as a PN-like diffuse object from a set of R and B plates. Although Kohoutek (2001) cataloged it as Possible PN, some studies in the literature for the last 20 years consider this object a galaxy, e.g., Paturel et al. (2003) identified it as an elliptical galaxy, Tempel et al. (2016) reported a photometric redshift of  $0.037633 \pm 0.000167$ , and a distance of 165.254 Mpc. HASH status is possible galaxy, SIMBAD status is PN candidate, and NED status is galaxy. Our spectrum shows no emission lines or apparent absorption features. Therefore, it is not possible to draw a more definitive conclusion.

*PN G358.4+08.9 (Terz N 29, LEDA 89010):* Terzan (1985) described it as a red star surrounded by nebulosity as it appeared in R and B plates. There are few studies in the literature, but Hasegawa et al. (2000) identify this object as a type E galaxy and report a redshift of  $0.027786 \pm 0.000167$ . Nevertheless, Kohoutek (2001) cataloged it as Possible PN. HASH status is a possible galaxy, SIMBAD status is PN candidate, and NED status is Galaxy. We have not found emission lines in our spectrum but several absorption features corresponding to G-band, Mg $\beta$ , NaD and H $\alpha$  typical of elliptical galaxies. We derived a redshift of  $z = 0.0279$  that is in complete agreement with previously reported value (Hasegawa et al. 2000).

*PN G058.6+00.9 (PN PM 1-309, IRAS 19353+2302):* Preite-Martinez (1988) proposed this object as a possible PN based on the far-IR colours of the source and reported density fluxes at 12, 25, 60, and 100  $\mu\text{m}$ . He calculated dust temperature assuming that is the unique source observed and estimated heliocentric distance (5.1 kpc).

## REFERENCES

- Acker, A., Marcout, J., Ochsenbein, F., Stenholm, B., Tylenda, R., & Schohn, C. 1992, The Strasbourg-ESO catalog of galactic planetary nebulae (Garching: ESO)
- Acker, A., et al. 2012, RMxAA, 48, 223
- Akras, S. & Gonçalves, D. R. 2016, MNRAS, 455, 930
- Ali, A., Dopita, M. A., Basurah, H. M., Amer, M. A., Alsulami, R., & Alruhaili, A. 2016, MNRAS, 462, 1393
- Ali, A. & Dopita, M. A. 2017, PASA, 34, e036
- Asplund, M., Amarsi, A. M., & Grevesse, N. 2021, A&A, 653, A141
- Bailer-Jones, C. A. L., Rybizki, J., Fouesneau, M., Demleitner, M., & Andrae, R. 2021, AJ, 161, 147
- Bojićić, I. S., Parker, Q. A., Filipović, M. D., & Frew, D. J. 2011, MNRAS, 412, 223
- Bojićić, I. S., Parker, Q. A., & Frew, D. J. 2017, in IAU Symposium, 323, Planetary Nebulae: Multi-Wavelength Probes of Stellar and Galactic Evolution, 327
- Boumis, P., et al. 2006, MNRAS, 367, 1551
- Cardelli, J. A., Clayton, G. C., & Mathis, J. S. 1989, ApJ, 345, 245
- Cesco, C. U. & Gibson, J. 1973, A&AS, 11, 335
- Chornay, N. & Walton, N. A. 2021, A&A, 656, A110
- Condon, J. J., Kaplan, D. L., & Terzian, Y. 1999, ApJS, 123, 219
- DePew, K., et al. 2011, MNRAS, 414, 2812
- Douchin, D., et al. 2015, MNRAS, 448, 3132
- Drew, J. E., et al. 2005, MNRAS, 362, 753
- Ferrero, L., Le Dû, P., Mulato, L., Outters, N., & Zoll, S. 2015, L'astronomie, 129, 42
- Frew, D. J. & Parker, Q. A. 2010, PASA, 27, 129
- Frew, D. J., Bojićić, I. S., & Parker, Q. A. 2013, MNRAS, 431, 2
- Frew, D. J., Parker, Q. A., & Bojićić, I. S. 2016, MNRAS, 455, 1459
- Froebrich, D., et al. 2015, MNRAS, 454, 2586
- Gaia Collaboration, et al. 2023, A&A, 674, A1
- Gentile Fusillo, N. P., et al. 2021, MNRAS, 508, 3877
- Gómez-Muñoz, M. A., Bianchi, L., & Manchado, A. 2023, ApJS, 266, 34
- González-Santamaría, I., Manteiga, M., Manchado, A., et al. 2021, A&A, 656, A51
- Hajduk, M., et al. 2021, ApJ, 919, 121
- Hambly, N. C., MacGillivray, H. T., Read, M. A., et al. 2001, MNRAS, 326, 1279
- Hasegawa, T., et al. 2000, MNRAS, 316, 326
- Henry, R. B. C., Kwinter, K. B., Jaskot, A. E., Balick, B., Morrison, M. A., & Milingo, J. B. 2010, ApJ, 724, 748
- Henry, R. B. C., Speck, A., Karakas, A. I., Ferland, G. J., & Maguire, M. 2012, ApJ, 749, 61
- Hsia, C.-H., & Zhang, Y. 2014, A&A, 563, 11
- Irabor, T., et al. 2018, MNRAS, 480, 2423
- Jacoby, G. H., et al. 2021, MNRAS, 506, 5223
- Kaler, J. B. & Jacoby, G. H. 1989, ApJ, 345, 871
- Kepler, S. O., et al. 2016, MNRAS, 455, 3413
- Kingsburgh, R. L. & Barlow, M. J. 1994, MNRAS, 271, 257
- Kohoutek, L. 2001, A&A, 378, 843
- Khushbu, K. & Muthumariappan, C. 2024, Advances in Space Research, 74, 1366
- Kwitter, K. B. & Henry, R. B. C. 2022, PASP, 134, 022001

- Kwok, S. 2000, The origin and evolution of planetary nebulae (New york: Cambridge university press)
- Le Dû, P., et al. 2022, A&A, 666, 10
- Maciel, W. J., Costa, R. D. D., & Idiart, T. E. P. 2010, A&A, 512, A19
- Makarov, D. I., Karachentsev, I. D., & Burenkov, A. N. 2003, A&A, 405, 951
- Mari, M. B., Akras, S., & Gonçalves, D. R. 2023, MNRAS, 525, 1998
- Miszalski B., Parker Q. A., Acker A., Birkby J. L., Frew D. J., & Kovacevic A. 2008, MNRAS, 384, 525
- Moe, M., & De Marco, O. 2006, ApJ, 650, 916
- Olgún, L., Vázquez, R., Contreras, M. E., & Jiménez, M. Y. 2011, RMxAC, 40, 193
- Osterbrock, D. E., & Ferland, J. G. 2006, The Astrophysics of Gaseous Nebulae and Active Galactic Nuclei (2nd. ed.; Sausalito: University science books)
- Parker, Q. A., Phillipps, S., Pierce, M. J., et al. 2005, MNRAS, 362, 689
- Parker, Q. A., et al. 2006, MNRAS, 373, 79
- Parker, Q. A., Bojičić, I., & Frew, D. 2016, JPCS, 728, 3
- Parker, Q. A. 2022, Frontiers in Astronomy and Space Sciences, 9, 895287
- Paturel, G., et al. 2003, A&A, 412, 45
- Peimbert, M. & Torres-Peimbert, S. 1983, in IAU Symposium, 103, Planetary Nebulae, 233
- Preite-Martinez, A. 1988, A&AS, 76, 317
- Quireza, C., Rocha-Pinto, H. J., & Maciel, W. J. 2007, A&A, 475, 217
- Raga, A. C., Riera, A., Meléma, G., Esquivel, A., & Velázquez, P. F. 2008, A&A, 489, 1141
- Ramos-Larios, G., Guerrero, M. A., Sabin, L., & Santamaría, E. 2017, MNRAS, 470, 3707
- Randall, S. K., Trejo, A., Humphreys, E. M. L., et al. 2020, A&A, 636, A123
- Reid, W. A. & Parker, Q. A. 2010, PASA, 27, 187
- Ritter, A., Parker, Q. A., Sabin, L., Le Dû, P., Mulato, L., & Patchick, D. 2023, MNRAS, 520, 773
- Robertson, T. H. & Jordan, T. M. 1989, AJ, 98, 1354
- Sabin, L., et al. 2014, MNRAS, 443, 3388
- Sabin, L., et al. 2021, MNRAS, 508, 1599
- Shaw, R.A. & Dufour, R. J. 1995, PASP, 107, 896
- Stanghellini, L., Guerrero, M. A., Cunha, K., Manchado, A., & Villaver, E. 2006, ApJ, 651, 898
- Stanghellini, L., Shaw, R. A., & Villaver, E. 2008, ApJ, 689, 194
- Tan, S., Parker, Q. A., Zijlstra, A. A., & Rees, B. 2024, MNRAS, 527, 6363
- Tempel, E., et al. 2016, A&A, 588, A14
- Temiz, U., et al. 2024, MNRAS, 527, 1481
- Terzan, A. 1985, The Messenger, 42, 4
- van de Steene, G. C., Jacoby, G. H., & Pottasch, S. R. 1996, A&AS, 118, 243
- Ueta, T., Mito, H., Otsuka, M., Nakada, Y., Conn, B. C. & Ladjal, D. 2019, AJ, 158, 145
- Urquhart, J. S., et al. 2009, A&A, 501, 539
- Viironen, K., et al. 2009, A&A, 502, 113
- Weidmann, W. A., et al. 2020, A&A, 640, A10
- York, D. G., Adelman, J., Anderson, J. E., et al. 2000, AJ, 120, 1579

- D. A. Belén-Molina, L. Olguín and M. E. Contreras: Departamento de Investigación en Física, Universidad de Sonora, Blvd. Rosales Esq. L.D. Colosio, Edif. 3H, 83000 Hermosillo, Son., Mexico (a219230153@unison.mx).
- L. F. Miranda: Instituto de Astrofísica de Andalucía – CSIC, Glorieta de la Astronomía s/n, E-18008 Granada, Spain.
- R. Vázquez: Instituto de Astronomía, Universidad Nacional Autónoma de México, Km 103 ctra. Tijuana-Ensenada, 22860 Ensenada, B.C., Mexico.